Supplemental Data

Ovarian cancer cell lines

Human ovarian adenocarcinoma OVCAR3 was purchased from American Type Culture Collection (ATCC). Human ovarian adenocarcinoma OVCAR4, OVCAR5, and OVCAR8 were purchased from the National Cancer Institute in 2020. All cell lines were authenticated by short tandem repeat (STR) profiling at Memorial Sloan Kettering (MSK) and were checked frequently for mycoplasma. Cultures were grown in aseptic conditions at 37°C and 5% CO_2 in a humidified atmosphere. OVCAR3 cells were grown in RPMI + 20% FCS, 10 mM HEPES, 2 mM L-Glutamine, 1 mM Sodium Pyruvate, 1.5 g/L sodium bicarbonate, 4.5 g/L glucose, 0.01 mg/mL bovine insulin, 100 units/mL penicillin, and 100 µg/mL streptomycin. OVCAR4, 5, and 8 cells were grown in RPMI 10% FCS, 2 mM L-glutamine, 100 units/mL penicillin, and 100 µg/mL streptomycin.

RNA Extraction & Quantitative real-time PCR (RT-PCR)

5 million cells were washed with PBS and pelleted prior to RNA extraction. The RNeasy mini kit (QIAGEN) was used to extract RNA. DNA digestion was performed using the RNase-Free DNase set (QIAGEN). RNA purity and quantity was determined using a Nanodrop-2000 to obtain the spectrophotometric values at 260 and 280 nm. qPCR was performed to quantify mRNA levels of *MUC16* in OVCAR3, 4, 5, and 8 cell lines. *MUC16* expression levels were normalized to their respective *actin* levels in each sample (ΔCq). Data was presented as fold change ($2\text{^}(-\Delta\Delta Cq)$), *MUC16* relative expression compared to OVCAR8. Cell pellets were lysed using QIAShredder and mRNA was extracted using a QIAGEN RNeasy isolation kit. Purified mRNA was converted to cDNA. Power SYBR Green was used for quantification. Triplicates were performed.

Bioconjugation and radiolabeling

^{89}Zr was purchased from 3D Imaging or produced by the Radiochemistry & Molecular Imaging Probes Core at MSK (21). [^{89}Zr]Zr-DFO-huAR9.6 was prepared using established procedures (22). The [^{89}Zr]Zr^{4+} chelator desferrioxamine (DFO) was conjugated to huAR9.6 with 6 molar equivalent of *p*-SCN-DFO (B-705; Macrocyclics, Inc) at 37°C for 1.5 h on a thermomixer. Reaction mixture was purified on a size-exclusion PD-10 desalting column (Cytiva). For radiolabeling, [^{89}Zr]Zr-oxalate was neutralized with 1M sodium carbonate (pH ~7) and was added to DFO-huAR9.6 in Chelex-treated PBS (pH 7). Reaction was placed on a thermomixer at 37°C for 1 h.

Lutetium-177 was purchased from Isotope Technologies Munich (ITM). [^{177}Lu]Lu-CHX-A"-DTPA-huAR9.6 was prepared by first conjugating the chelator CHX-A"-DTPA to huAR9.6 with 6-molar-equivalent of *p*-SCN-CHX-A"-DTPA (B-355; Macrocyclics, Inc). Reaction mixture was purified on a size exclusion PD-10 desalting column (Cytiva). For radiolabeling, ^{177}Lu was combined with CHX-A"-DTPA-huAR9.6 in Chelex-treated ammonium acetate (pH 5.5, 0.25 M) at 37°C for 1 h on a thermomixer. Purity for all ^{89}Zr- and ^{177}Lu-radiolabeling studies was assessed with radio-instant thin layer chromatography (radio-iTLC) using 50 mM ethylenediaminetetraacetic acid (EDTA) for the eluent.

Saturation Binding Assay

[^{89}Zr]Zr-DFO-huAR9.6 was prepared (500 µg/mL) in PBS with 1% BSA. Serial dilutions of the radiolabeled antibody were added to each tube containing 1M OVCAR3 cells in media. [^{177}Lu]Lu-CHX-A"-DTPA-huAR9.6 was prepared (210 µg/mL) in PBS with 1% BSA. Serial dilutions of the radiolabeled antibody were added to each tube containing 0.5M OVCAR3 cells in media.

The cells were incubated with the radiolabeled antibody for 1 hour. The cells were then washed with ice-cold PBS three times using a Brandel Cell Harvester on to Whatman GF/B filter paper, CAT: FP-100. The

filter paper (containing cells) was added to a biodistribution tube and placed on gamma counter for *ex vivo* quantification of radioligand binding. Non-specific binding was calculated by incubating media without cells with the radiotracer and conducting the subsequent washes on the filter paper.

In vitro Bead Binding Assay

Recombinant biotinylated MUC16 protein (ACROBiosystems; 1 µg) was incubated with Streptavidin magnetic beads (R&D systems) in protein Lo-Bind Eppendorf tubes for 15 minutes. [^{89}Zr]Zr-DFO-huAR9.6 (1 ng) was then added to each Eppendorf tube and incubated at 4°C for 1 hour. For the control arm, [^{89}Zr]Zr-DFO-huAR9.6 was incubated with the streptavidin beads without biotinylated MUC16. The blocking arm contained an excess of unlabeled DFO-huAR9.6 (3 µg). Beads were washed three times after incubation with radioligand. The beads, supernatant, and three wash fractions were analyzed on a gamma counter to determine the percentage of radiolabeled huAR9.6 bound to each fraction (23).

In vitro Cell Binding Assays

[^{89}Zr]Zr-DFO-huAR9.6 or [^{177}Lu]Lu-CHX-A"-DTPA-huAR9.6 in PBS with 1% BSA (0.15 µg/mL; 3 ng) was added to Eppendorf tubes containing 1 M cells per replicate and incubated on ice for 1 hour with intermittent mixing. The blocking arms contained a 1000-fold excess of unlabeled huAR9.6. Cells were centrifuged (600 x g for 5 min) and supernatant was collected. Cells were then washed with ice-cold PBS (3x). Cells were centrifuged and collected. The cell pellet, supernatant, and three wash fractions were placed on a gamma counter for *ex vivo* quantification of binding.

Flow Cytometry

Flow cytometry was used to determine the MUC16-binding affinity of huAR9.6 with the OVCAR3, OVCAR4, OVCAR5, and OVCAR8 cell lines. Unstained cells were used as a control. Cells (10^6) were incubated with FcR block (Miltenyi Biotec) for 15 minutes on ice. Cells were then incubated with 5 mg/mL of conjugated huAR9.6-AlexaFluor488 (1:200 dilution) for 40 minutes at 4°C followed by rinses with ice cold FACS buffer. A 1:1000 dilution of 4′,6-diamidino-2-phenylindole (DAPI) (Sigma Aldrich) was used to exclude dead cells. Samples were analyzed on a BD LSR Fortessa and data processed with FlowJo v10.

Serum Stability

The *in vitro* stability of [^{89}Zr]Zr-DFO-huAR9.6 and [^{177}Lu]Lu-CHX-A"-DTPA-huAR9.6 was tested for demetallation of [^{89}Zr]Zr^{4+} or [^{177}Lu]Lu^{3+}. Both radioimmunoconjugates were incubated individually in human AB-type serum (H4522; Sigma Aldrich). 1.85 MBq (5 µg) of each radioimmunoconjugate having a specific activity of ~ 0.37 MBq/µg was incubated with 1 mL of human serum and placed on a thermomixer set at 37 °C. Triplicate samples were used for each radioimmunoconjugate. Each sample was analyzed via radio-iTLC. 1 µL of each sample was spotted on the baseline of a silica-gel paper strip. The strips were dipped into a vertical TLC chamber containing EDTA (50 mM, pH = 5.5) as the mobile phase. After the solvent traveled to the top of the strips, the strips were analyzed by placing them on an AR-2000 iTLC scanner (Bioscan Inc., Washington, DC). Area under the curves for the peak at the baseline in comparison to the solvent front peak were recorded. This process was repeated every day for up to 7 days post-incubation. Serum stability is reported as % intact which indicates the percentage of [^{89}Zr]Zr^{4+} or [^{177}Lu]Lu^{3+} that stays bound to huAR9.6. Intact radioimmunoconjugates will stay at the baseline.

Immunohistochemistry

Tumor tissue samples were harvested and fixed in 10% neutral buffered formalin. Fixed tissues were processed and embedded in paraffin blocks. Sections were taken from paraffin-embedded blocks. Slides were stained with hematoxylin and eosin (H&E) or used for immunohistochemistry by the Laboratory of Comparative Pathology at MSK. Slides were heated at 58–60ºC for 30 min followed by deparaffinizing in xylene and hydrated in graded alcohols and water. Tissue sections were blocked for 15 min with 1% hydrogen peroxide in PBS.

Primary anti-MUC16 antibody (huAR9.6) was diluted at 1:100 with 2% BSA–PBS and incubated on the slides overnight at 4ºC. After rinsing, biotinylated goat anti-mouse IgG (1:500 diluted in 1% BSA-PBS; Vector Labs, Cat. No. BA-2000) was incubated on the slides for 60 min at room temperature followed by application of the Avidin-Biotin Complex Elite kit (Vector Labs, Cat. No. PK-6100). 3,3'-Diaminobenzidine substrate (Fisher, Cat. No. AAH5400014) was added to the slides and then the slides were counterstained with hematoxylin and coverslipped with Permount (Fisher Scientific).

Dosimetry

Dosimetry estimates for [^{177}Lu]Lu-DTPA-huAR9.6 were obtained from the *ex vivo* biodistribution data in OVCAR3 xenografted mice. Uptake in the blood was assumed to be representative of uptake in the hematopoietic bone marrow; uptake in muscle tissue was assumed to be representative of tissues not harvested for *ex vivo* gamma counting biodistribution measurements. The %ID/g organ uptake values were converted to standardized uptake values (SUVs; normalized by total body mass) and transposed into representative mouse and representative human computational phantoms for dosimetry computations. The percentage of injected dose in phantom organ I, $\%ID_I$, was obtained from Eqn. S1, which assumes SUV is independent of body mass:

$$\%ID_I = SUV_i \cdot \frac{m_I}{m_{TB}} \times 100\% \qquad \text{Eqn. S1}$$

where SUV_i is the standardized uptake value for mouse organ i, m_I is the mass of corresponding phantom organ I, and m_{TB} is the total phantom mass. The $\%ID_I$ at each time point was subsequently multiplied by a corresponding radioactive decay factor to obtain *effective* time-activity curves (i.e., entailing both radioactive decay and biological clearance). Effective activity-time curves were fit with either a monoexponential (decay) of the form:

$$\%ID_I = Ae^{-at} \qquad \text{Eqn. S2}$$

or biexponential (uptake and clearance) model of the form:

$$\%ID_I = A(e^{-at} - e^{-bt}) \qquad \text{Eqn. S3}$$

via weighted least squares nonlinear regression using the Microsoft Excel SOLVERSTAT statistics package (24). The optimized model parameters were used along with the analytical expressions for the integrals of the fit functions to obtain time-integrated activity coefficients (TIACs in units of h) (25).

Absorbed dose coefficients for murine organs were calculated using the 25g reference mouse (MOBY phantom) within PARaDIM 1.0/PHITS version 3.20 (26, 27). All PARaDIM parameter defaults for electron and photon transport were used; 2×10^7 total events were simulated, resulting in <2% statistical uncertainty in the organ-level dose coefficients. Absorbed dose coefficients for human organs were calculated using the International Commission on Radiological Protection (ICRP) human female reference phantom within MIRDcalc software (28).

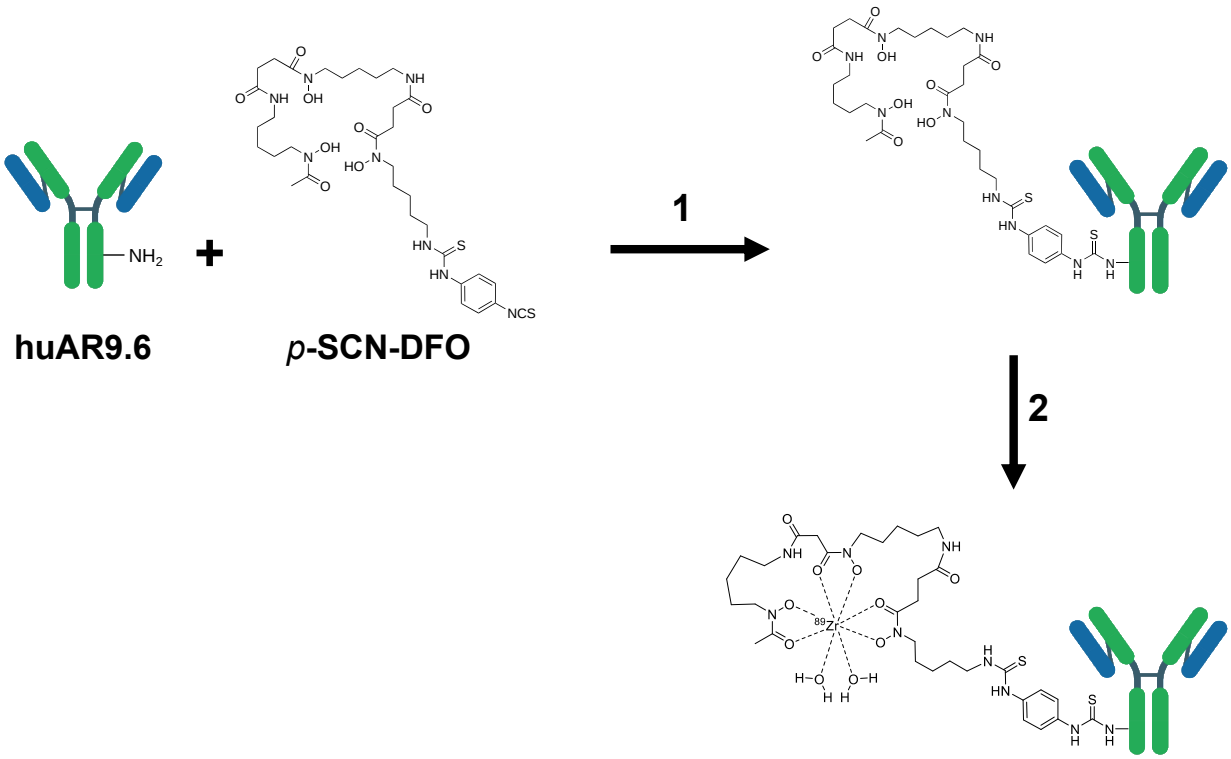

Supplemental Figure 1. Synthesis overview of [^{89}Zr]Zr-DFO-huAR9.6. Schematic representation of [^{89}Zr]Zr-DFO-huAR9.6 showing the bioconjugation of the chelator, DFO, to huAR9.6, followed by radiolabeling of huAR9.6-DFO. (1) Chelex-treated PBS, pH 8.8, 37°C, 90 min; (2) [^{89}Zr]Zr-oxalate, Chelex-treated PBS, pH 6.8, 37°C, 60 min.

A

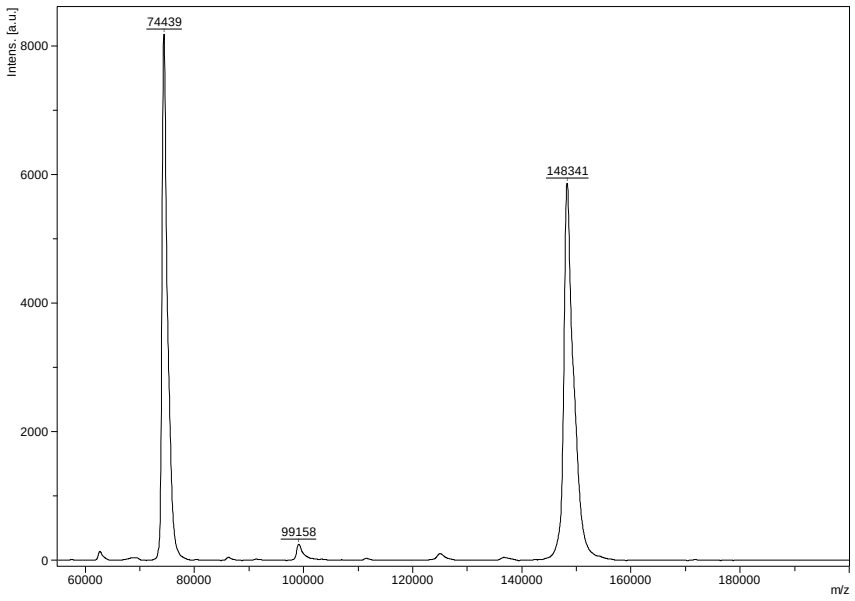

B

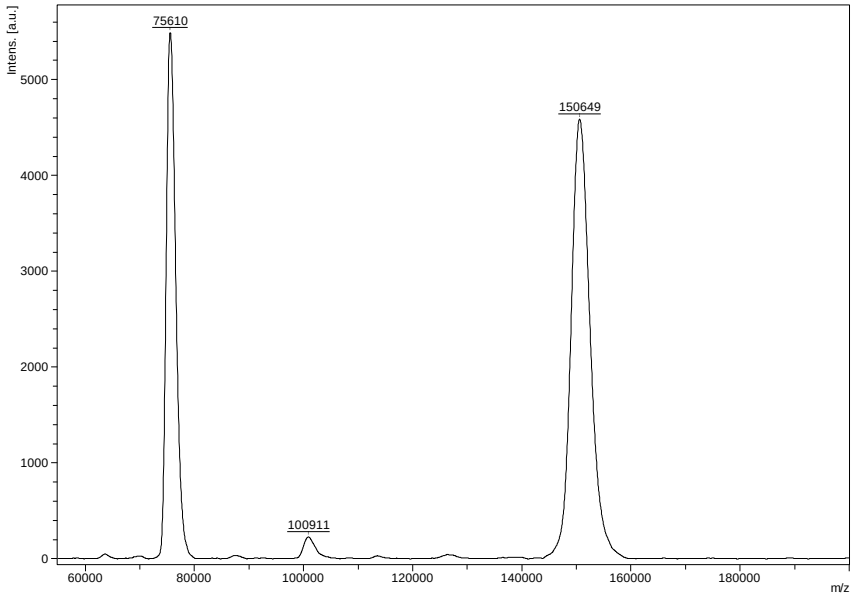

Supplemental Figure 2. MALDI-TOF spectra of unmodified and modified huAR9.6. (A) Unmodified huAR9.6 shows a peak at MW ~148341 with the **(B)** huAR9.6-DFO peak at MW ~150649, which calculates to an average of ~3 DFO molecules per antibody.

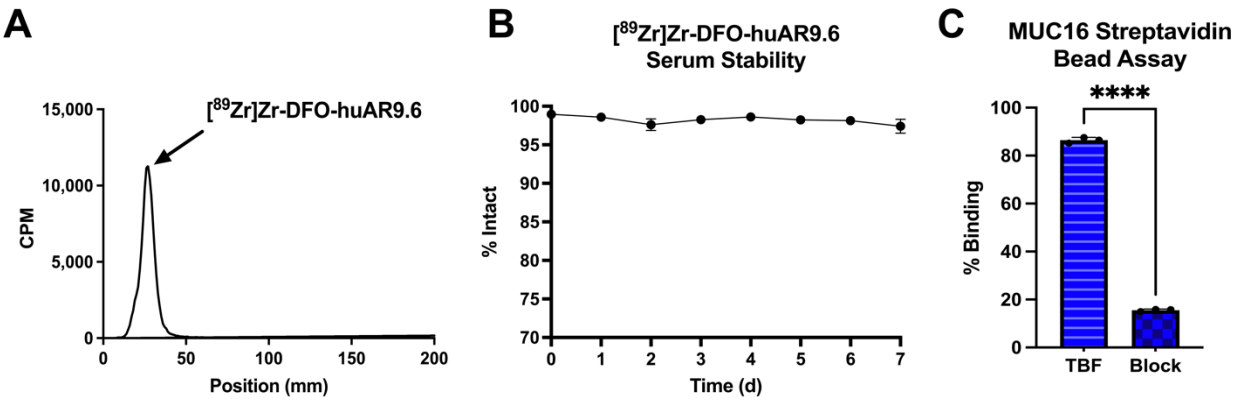

Supplemental Figure 3. *In vitro* characterization of [^{89}Zr]Zr-DFO-huAR9.6. (A) Radio-instant thin layer chromatography of [^{89}Zr]Zr-DFO-huAR9.6 showing high radiochemical purity > 99%. **(B)** [^{89}Zr]Zr-DFO-huAR9.6 shows >95% stability in human serum over 7 days at 37ºC. **(C)** *In vitro* MUC16 bead-binding [^{89}Zr]Zr-DFO-huAR9.6 shows high and specific binding to MUC16 beads at ~85%. Binding is blockable with a 1000-fold excess of unlabeled huAR9.6.

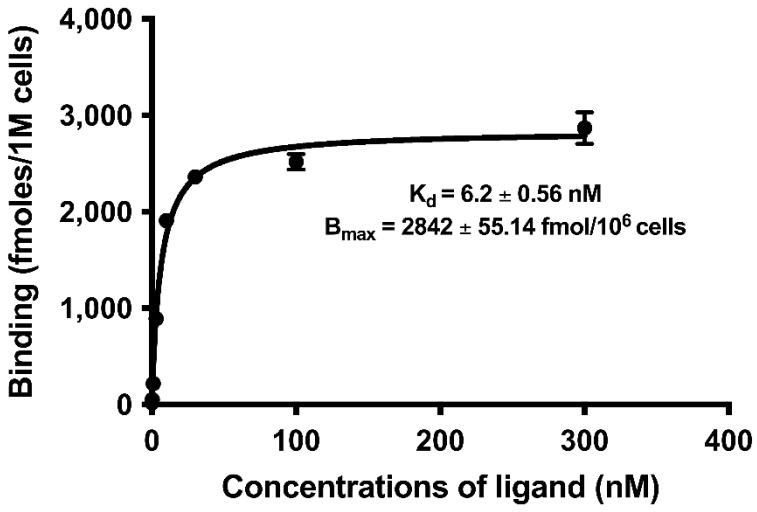

Supplemental Figure 4. Saturation binding curve of [^{89}Zr]Zr-DFO-huAR9.6 to OVCAR3 cells. PRISM v8 was used to calculate the B_{max} of 2842 ± 55.14 femtomoles/10^6 cells and a K_d of 6.2 nM.

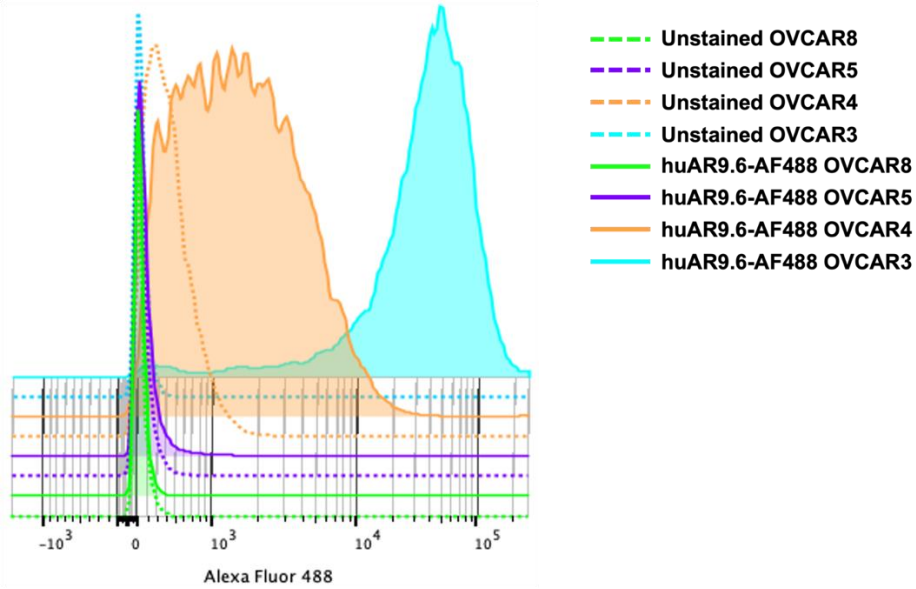

Supplemental Figure 5. Flow cytometry analysis with huAR9.6-AF488 in ovarian cancer cell lines. *In vitro* flow cytometry analysis of the binding of huAR9.6-AF488 to MUC16^{high} OVCAR3, MUC16^{high} OVCAR4, MUC16^{low} OVCAR5, and MUC16^{negative} OVCAR8 cells.

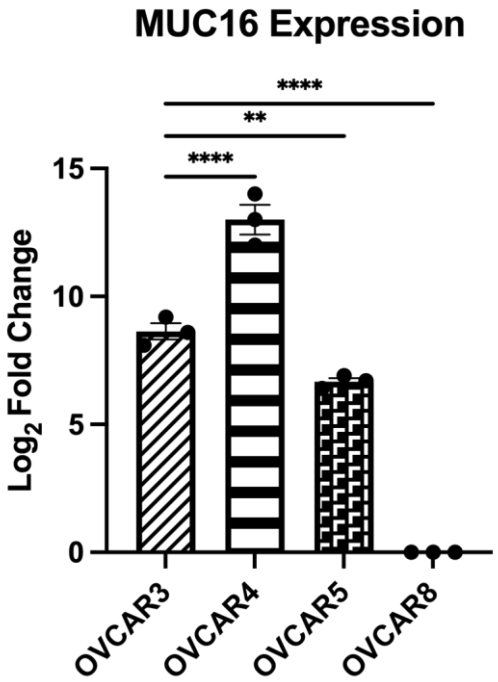

Supplemental Figure 6. Real-time polymerase chain reaction shows mRNA expression levels of *MUC16* in the OVCAR3, 4, and 5 cells line in comparison to the MUC16-negative OVCAR8 as control. **P*-value ≤ 0.05, ***P*-value ≤ 0.01, ****P*-value ≤ 0.001, *****P*-value ≤ 0.0001.

Xenograft / Tissues	OVCAR3 (n=4)	OVCAR4 (n=3)	OVCAR5 (n=4)	OVCAR8 (n=3)
Blood	0.43 ± 0.22	3.74 ± 1.57	3.46 ± 1.63	1.84 ± 1.23
Heart	0.47 ± 0.10	1.47 ± 0.57	1.15 ± 0.37	0.73 ± 0.08
Lungs	1.18 ± 0.21	2.63 ± 0.74	2.46 ± 0.72	1.33 ± 0.57
Liver	13.68 ± 1.36	12.27 ± 1.19	10.38 ± 2.59	8.34 ± 2.46
Spleen	9.2 ± 1.72	17.72 ± 8.28	9.56 ± 4.07	9.72 ± 9.59
Pancreas	0.41 ± 0.11	0.61 ± 0.09	0.47 ± 0.14	0.65 ± 0.21
Stomach	0.53 ± 0.26	0.63 ± 0.20	0.61 ± 0.37	0.13 ± 0.04
Small Intestine	0.63 ± 0.43	0.64 ± 0.20	0.33 ± 0.09	0.54 ± 0.47
Large Intestine	0.54 ± 0.12	0.44 ± 0.14	0.47 ± 0.28	0.25 ± 0.10
Kidneys	2.57 ± 0.26	2.48 ± 0.19	2.35 ± 0.51	1.92 ± 0.16
Muscle	0.18 ± 0.01	0.43 ± 0.09	0.69 ± 0.42	0.24 ± 0.07
Bone	3.01 ± 0.58	1.99 ± 0.31	2.41 ± 0.73	2.40 ± 2.42
Skin	1.19 ± 0.28	1.79 ± 0.24	2.26 ± 0.60	1.18 ± 0.21
Tumor	35.17 ± 4.99	23.87 ± 6.37	13.46 ± 3.80	1.46 ± 0.10
Tail	0.63 ± 0.09	2.48 ± 1.21	1.10 ± 0.15	0.72 ± 0.21

Supplemental Figure 7. Tabulated *ex vivo* biodistribution data 144 hours after lateral tail vein injection of [^{89}Zr]Zr-DFO-huAR9.6 in OVCAR3, OVCAR4, OVCAR5, and OVCAR8 tumor-bearing female nude mice (20–25 µg, 7.4 – 9.25 MBq). Data expressed as mean percent injected dose per gram (%ID/g ± SD). Spleen sizes for OVCAR4 group were significantly smaller in comparison to OVCAR3, 5, and 8 groups.

A

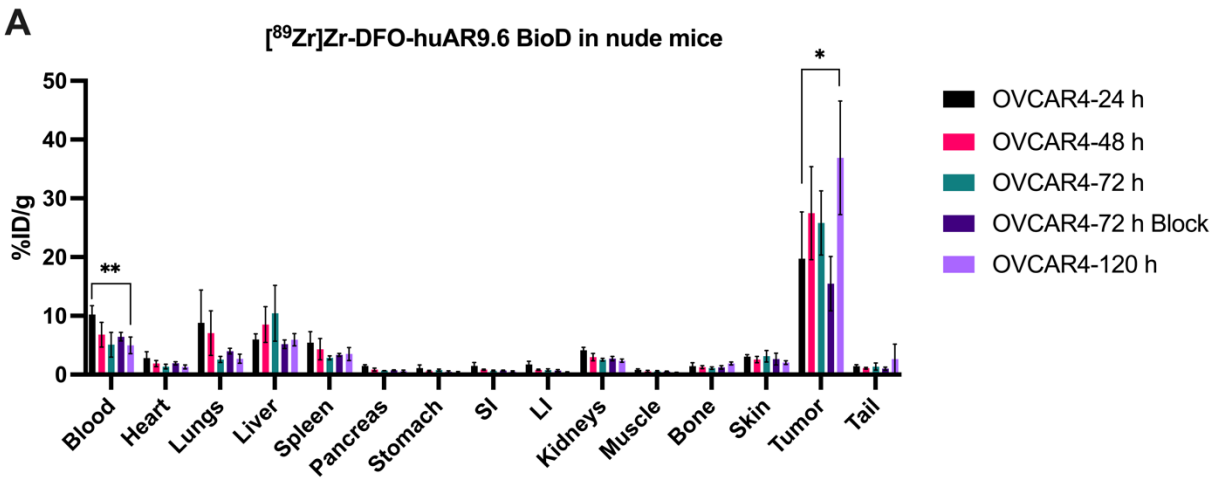

B

Time (p.i.) / Tissues	24 h (n=4)	48 h (n=4)	72 h (n=4)	72 h-Blk (n=4)	96 h (n=4)	120 h (n=4)
Blood	10.25 ± 1.48	6.80 ± 2.10	5.09 ± 2.11	6.45 ± 0.72	2.73 ± 2.25	4.97 ± 1.42
Heart	2.83 ± 1.05	1.88 ± 0.53	1.37 ± 0.41	1.92 ± 0.26	0.83 ± 0.47	1.30 ± 0.34
Lungs	8.81 ± 5.58	7.07 ± 3.81	2.58 ± 0.52	3.99 ± 0.47	1.75 ± 1.08	2.71 ± 0.79
Liver	5.97 ± 0.95	8.51 ± 3.05	10.44 ± 4.74	5.17 ± 0.71	10.53 ± 4.05	5.94 ± 1.05
Spleen	5.44 ± 1.89	4.33 ± 1.80	2.85 ± 0.34	3.37 ± 0.24	6.76 ± 3.55	3.51 ± 1.10
Pancreas	1.48 ± 0.21	0.87 ± 0.25	0.67 ± 0.03	0.75 ± 0.09	0.48 ± 0.25	0.60 ± 0.17
Stomach	1.11 ± 0.54	0.59 ± 0.13	0.78 ± 0.18	0.47 ± 0.17	0.26 ± 0.11	0.40 ± 0.13
Small Intestine	1.47 ± 0.57	0.84 ± 0.10	0.66 ± 0.12	0.68 ± 0.09	0.60 ± 0.47	0.53 ± 0.12
Large Intestine	1.72 ± 0.55	0.83 ± 0.10	0.79 ± 0.18	0.71 ± 0.17	0.51 ± 0.22	0.40 ± 0.08
Kidneys	4.14 ± 0.53	2.97 ± 0.63	2.53 ± 0.24	2.73 ± 0.37	2.15 ± 0.70	2.37 ± 0.27
Muscle	0.83 ± 0.17	0.56 ± 0.18	0.55 ± 0.13	0.51 ± 0.10	0.25 ± 0.09	0.36 ± 0.04
Bone	1.43 ± 0.58	1.27 ± 0.25	1.11 ± 0.21	1.23 ± 0.28	2.37 ± 2.17	1.90 ± 0.26
Skin	3.05 ± 0.34	2.56 ± 0.53	3.13 ± 0.98	2.65 ± 1.00	1.50 ± 0.64	2.05 ± 0.31
Tumor	19.74 ± 7.93	27.49 ± 7.91	25.81 ± 5.45	15.47 ± 4.62	23.65 ± 4.88	36.89 ± 9.68
Tail	1.44 ± 0.25	1.09 ± 0.15	1.36 ± 0.60	1.01 ± 0.26	0.84 ± 0.35	2.67 ± 2.51

Supplemental Figure 8. Full *ex vivo* biodistribution data after lateral tail vein injection of [^{89}Zr]Zr-DFO-huAR9.6 in OVCAR4 tumor-bearing nude mice (3µg, 1.11–1.30 MBq). **(A)** Percent injected dose per gram (%ID/g) 24-, 48-, 72-, and 120-hour timepoints. **(B)** Tabulated *ex vivo* biodistribution data. Expressed as mean percent injected dose per gram (%ID/g ± SD). **P*-value ≤ 0.05, ***P*-value ≤ 0.01, ****P*-value ≤ 0.001, *****P*-value ≤ 0.0001.

A

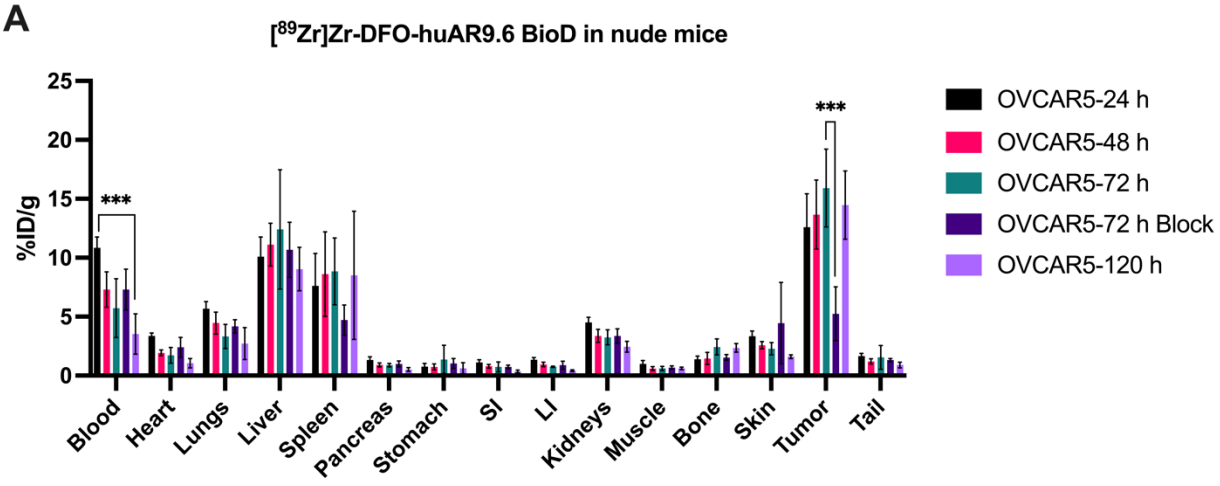

B

Time (p.i.) / Tissues	24 h (n=4)	48 h (n=4)	72 h (n=4)	72 h-Blk (n=4)	96 h (n=3)	120 h (n=4)
Blood	10.84 ± 0.93	7.30 ± 1.50	5.73 ± 2.49	7.31 ± 1.73	2.34 ± 1.77	3.53 ± 1.72
Heart	3.35 ± 0.25	1.93 ± 0.24	1.71 ± 0.67	2.40 ± 0.84	0.68 ± 0.36	1.06 ± 0.39
Lungs	5.68 ± 0.60	4.46 ± 0.93	3.32 ± 1.01	4.18 ± 0.56	1.62 ± 0.76	2.72 ± 1.36
Liver	10.10 ± 1.66	11.11 ± 1.81	12.41 ± 5.07	10.68 ± 2.33	15.04 ± 7.54	9.04 ± 1.84
Spleen	7.61 ± 2.75	8.61 ± 3.58	8.84 ± 2.83	4.72 ± 1.28	17.36 ± 2.12	8.51 ± 5.44
Pancreas	1.32 ± 0.27	0.91 ± 0.17	0.89 ± 0.15	0.99 ± 0.25	0.49 ± 0.07	0.52 ± 0.16
Stomach	0.76 ± 0.27	0.73 ± 0.25	1.37 ± 1.19	1.03 ± 0.42	0.57 ± 0.21	0.63 ± 0.47
Small Intestine	1.12 ± 0.21	0.80 ± 0.16	0.74 ± 0.42	0.73 ± 0.15	0.48 ± 0.10	0.35 ± 0.12
Large Intestine	1.34 ± 0.18	0.94 ± 0.19	0.75 ± 0.05	0.88 ± 0.34	0.41 ± 0.12	0.42 ± 0.07
Kidneys	4.50 ± 0.45	3.37 ± 0.56	3.25 ± 0.64	3.36 ± 0.60	2.05 ± 0.36	2.45 ± 0.45
Muscle	1.00 ± 0.27	0.60 ± 0.16	0.611 ± 0.18	0.67 ± 0.15	0.32 ± 0.13	0.61 ± 0.11
Bone	1.39 ± 0.27	1.45 ± 0.51	2.44 ± 0.68	1.54 ± 0.24	1.61 ± 0.14	2.35 ± 0.37
Skin	3.33 ± 0.45	2.58 ± 0.31	2.28 ± 0.52	4.46 ± 3.44	1.11 ± 0.41	1.61 ± 0.16
Tumor	12.60 ± 2.82	13.66 ± 2.93	15.91 ± 3.30	5.25 ± 2.29	11.81 ± 2.36	14.46 ± 2.89
Tail	1.65 ± 0.23	1.21 ± 0.23	1.54 ± 1.02	1.32 ± 0.13	0.67 ± 0.14	0.90 ± 0.23

Supplemental Figure 9. Full *ex vivo* biodistribution data after lateral tail vein injection of [^{89}Zr]Zr-DFO-huAR9.6 in OVCAR5 tumor-bearing nude mice (3 µg, 1.07–1.18 MBq). **(A)** Percent injected dose per gram (%ID/g) 24-, 48-, 72-, and 120-hour timepoints. Tumor uptake was blockable at 72-hour post injection with a co-injection of 100-fold excess unlabeled huAR9.6. **(B)** Tabulated *ex vivo* biodistribution data. Expressed as mean percent injected dose per gram (%ID/g ± SD). **P*-value ≤ 0.05, ***P*-value ≤ 0.01, ****P*-value ≤ 0.001, *****P*-value ≤ 0.0001.

A

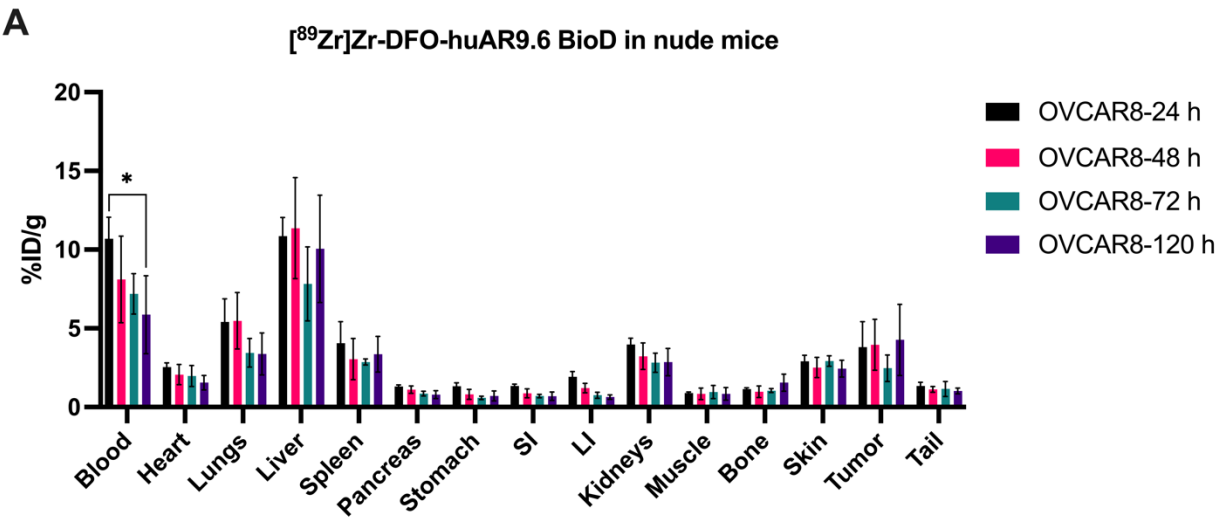

B

Time (p.i.) / Tissues	24 h (n=4)	48 h (n=4)	72 h (n=4)	96 h (n=4)	120 h (n=4)
Blood	10.69 ± 1.38	8.11 ± 2.75	7.19 ± 1.29	5.41 ± 1.57	5.87 ± 2.47
Heart	2.54 ± 0.26	2.06 ± 0.64	1.98 ± 0.67	1.57 ± 0.11	1.55 ± 0.46
Lungs	5.40 ± 1.48	5.48 ± 1.80	3.45 ± 0.91	2.77 ± 0.26	3.37 ± 1.33
Liver	10.87 ± 1.17	11.37 ± 3.21	7.82 ± 2.35	11.61 ± 1.84	10.06 ± 3.41
Spleen	4.06 ± 1.37	3.04 ± 1.31	2.87 ± 0.18	3.30 ± 0.89	3.35 ± 1.14
Pancreas	1.30 ± 0.10	1.11 ± 0.24	0.86 ± 0.15	0.64 ± 0.04	0.80 ± 0.25
Stomach	1.33 ± 0.22	0.80 ± 0.32	0.59 ± 0.11	0.59 ± 0.18	0.71 ± 0.31
Small Intestine	1.35 ± 0.12	0.88 ± 0.28	0.70 ± 0.11	0.59 ± 0.10	0.70 ± 0.27
Large Intestine	1.93 ± 0.33	1.20 ± 0.30	0.75 ± 0.19	0.59 ± 0.11	0.64 ± 0.14
Kidneys	3.98 ± 0.40	3.23 ± 0.84	2.82 ± 0.61	2.48 ± 0.28	2.86 ± 0.86
Muscle	0.88 ± 0.08	0.84 ± 0.36	0.95 ± 0.42	0.54 ± 0.03	0.84 ± 0.40
Bone	1.15 ± 0.07	0.97 ± 0.37	1.05 ± 0.12	1.21 ± 0.28	1.55 ± 0.54
Skin	2.91 ± 0.38	2.51 ± 0.64	2.92 ± 0.34	2.59 ± 0.51	2.44 ± 0.54
Tumor	3.82 ± 1.60	3.95 ± 1.62	2.47 ± 0.84	3.14 ± 0.34	4.27 ± 2.26
Tail	1.34 ± 0.24	1.12 ± 0.19	1.15 ± 0.47	0.96 ± 0.18	1.03 ± 0.18

Supplemental Figure 10. Full *ex vivo* biodistribution data after lateral tail vein injection of [^{89}Zr]Zr-DFO-huAR9.6 in OVCAR8 tumor-bearing nude mice (3 µg, 1.11–1.30 MBq). **(A)** Percent injected dose per gram (%ID/g) 24-, 48-, 72-, and 120-hour timepoints. **(B)** Tabulated *ex vivo* biodistribution data. Expressed as mean percent injected dose per gram (%ID/g ± SD). **P*-value ≤ 0.05, ***P*-value ≤ 0.01, ****P*-value ≤ 0.001, *****P*-value ≤ 0.0001.

A

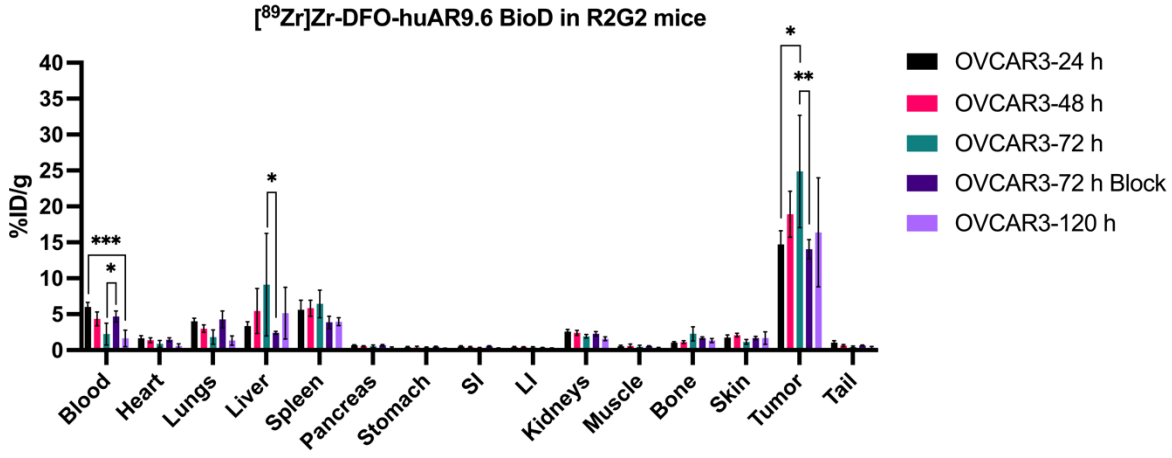

B

Time (p.i.) / Tissues	24 h (n=4)	48 h (n=4)	72 h (n=4)	72 h-Blk (n=4)	96 h (n=4)	120 h (n=4)	144 h (n=4)
Blood	6.01 ± 0.63	4.34 ± 0.97	2.24 ± 1.52	4.69 ± 0.77	1.75 ± 1.44	1.64 ± 1.16	1.11 ± 0.71
Heart	1.65 ± 0.36	1.38 ± 0.34	0.89 ± 0.46	1.45 ± 0.27	0.65 ± 0.51	0.57 ± 0.33	0.48 ± 0.24
Lungs	4.01 ± 0.44	2.99 ± 0.51	1.83 ± 1.00	4.29 ± 1.17	1.31 ± 0.93	1.34 ± 0.64	1.00 ± 0.42
Liver	3.34± 0.60	5.44 ± 3.14	9.17 ± 7.14	2.43 ± 0.20	7.38 ± 3.62	5.15 ± 3.59	4.88 ± 1.12
Spleen	5.61 ± 1.33	5.83 ± 1.12	6.44 ± 1.92	3.88 ± 0.84	4.22 ± 1.57	3.95 ± 0.55	15.78 ± 5.28
Pancreas	0.68 ± 0.06	0.54 ± 0.08	0.54 ± 0.19	0.68 ± 0.09	0.45 ± 0.25	0.32 ± 0.13	0.22 ± 0.09
Stomach	0.43 ± 0.08	0.39 ± 0.17	0.37 ± 0.09	0.48 ± 0.05	0.28 ± 0.15	0.20 ± 0.07	0.24 ± 0.07
Small Intestine	0.52 ± 0.08	0.43 ± 0.10	0.31 ± 0.08	0.54 ± 0.07	0.21 ± 0.10	0.21 ± 0.10	0.18 ± 0.06
Large Intestine	0.43 ± 0.08	0.44 ± 0.05	0.37 ± 0.13	0.35 ± 0.04	0.19 ± 0.07	0.23 ± 0.10	0.19 ± 0.02
Kidneys	2.57 ± 0.29	0.59 ± 0.25	1.93 ± 0.26	2.28 ± 0.32	1.68 ± 0.52	1.58 ± 0.28	1.49 ± 0.20
Muscle	0.57 ± 0.13	1.12 ± 0.18	0.48 ± 0.21	0.55 ± 0.08	0.29 ± 0.11	0.29 ± 0.08	0.17 ± 0.06
Bone	1.04 ± 0.15	2.09 ± 0.25	2.27 ± 0.98	1.69 ± 0.16	1.10 ± 0.42	1.33 ± 0.29	2.20 ± 0.42
Skin	1.76 ± 0.35	2.09 ± 0.25	1.14 ± 0.32	1.67 ± 0.23	1.61 ± 0.78	1.69 ± 0.86	1.24 ± 0.67
Tumor	14.71 ± 1.91	18.92 ± 3.19	24.88 ± 7.82	14.05 ± 1.33	19.42 ± 5.05	16.39 ± 7.58	16.09 ± 3.32
Tail	1.04 ± 0.27	0.63 ± 0.13	0.46 ± 0.12	0.65 ± 0.05	0.43 ± 0.22	0.35 ± 0.17	0.31 ± 0.08

Supplemental Figure 11. Full *ex vivo* biodistribution data after lateral tail vein injection of [^{89}Zr]Zr-DFO-huAR9.6 in OVCAR3 tumor-bearing R2G2 mice (3 µg, 0.93–1.18 MBq). **(A)** Percent injected dose per gram (%ID/g) 24-, 48-, 72-, and 120-hour timepoints. Tumor uptake was blockable at 72-hour post injection with a co-injection of 100-fold excess unlabeled huAR9.6. **(B)** Tabulated *ex vivo* biodistribution data. Expressed as mean percent injected dose per gram (%ID/g ± SD). 144-hour column represents terminal biodistribution from imaging cohort (20 µg, 7.77–8.88 MBq). **P*-value ≤ 0.05, ***P*-value ≤ 0.01, ****P*-value ≤ 0.001, *****P*-value ≤ 0.0001.

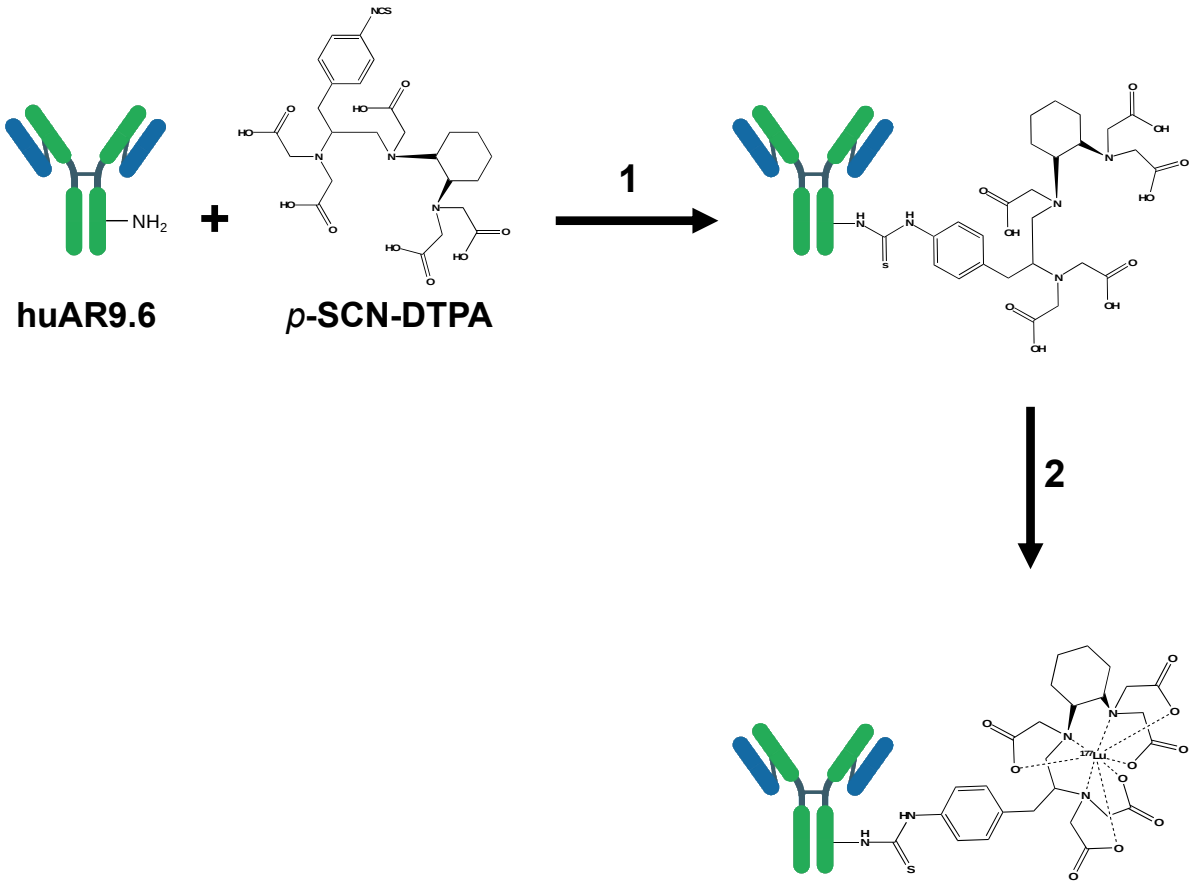

Supplemental Figure 12. Synthesis overview of [^{177}Lu]Lu-CHX-A"-DTPA-huAR9.6. Schematic representation of [^{177}Lu]Lu-CHX-A"-DTPA-huAR9.6 showing the bioconjugation of the chelator, CHX-A"-DTPA, to huAR9.6. Followed by radiolabeling of huAR9.6-DTPA. (1) Chelex-treated PBS, pH 8.8, 37°C, 90 min; (2) [^{177}Lu]$LuCl_3$, Chelex-treated NH_4OAc buffer, pH 5.5, 37°C, 60 min.

A

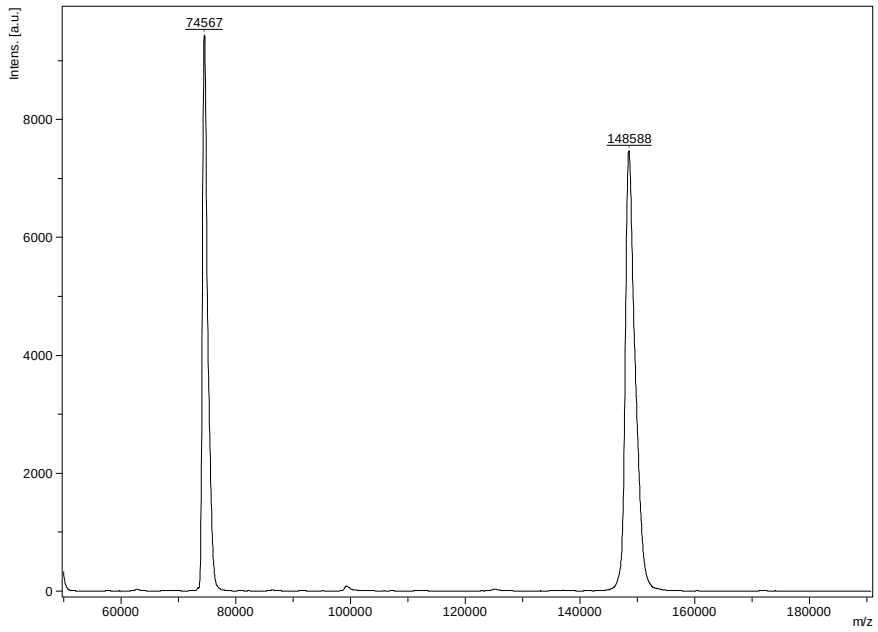

B

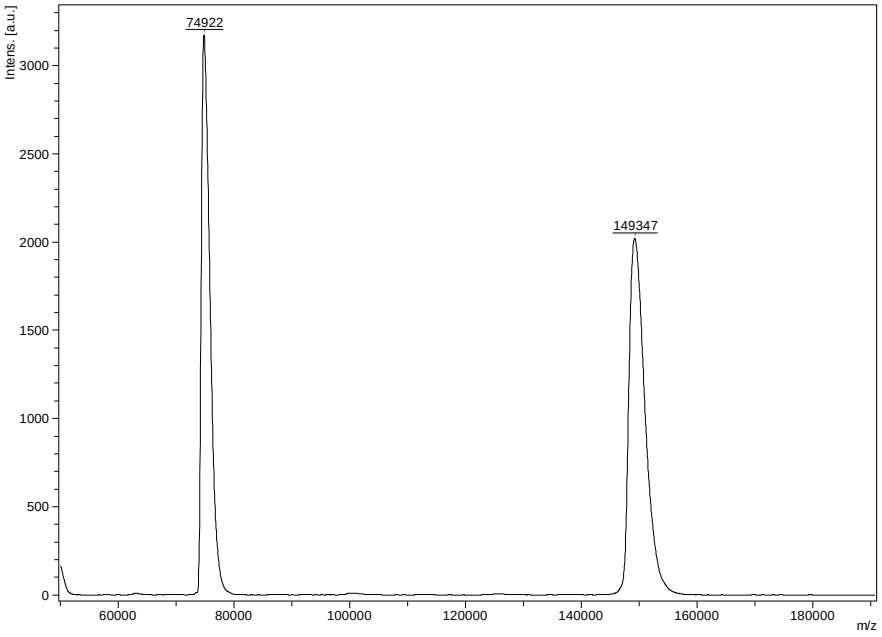

Supplemental Figure 13. MALDI-TOF spectra of unmodified and modified huAR9.6. (A) Unmodified huAR9.6 shows a peak at MW ~148588 with the **(B)** huAR9.6-DTPA peak at MW ~149347, which calculates to an average of ~1 DTPA molecule per antibody.

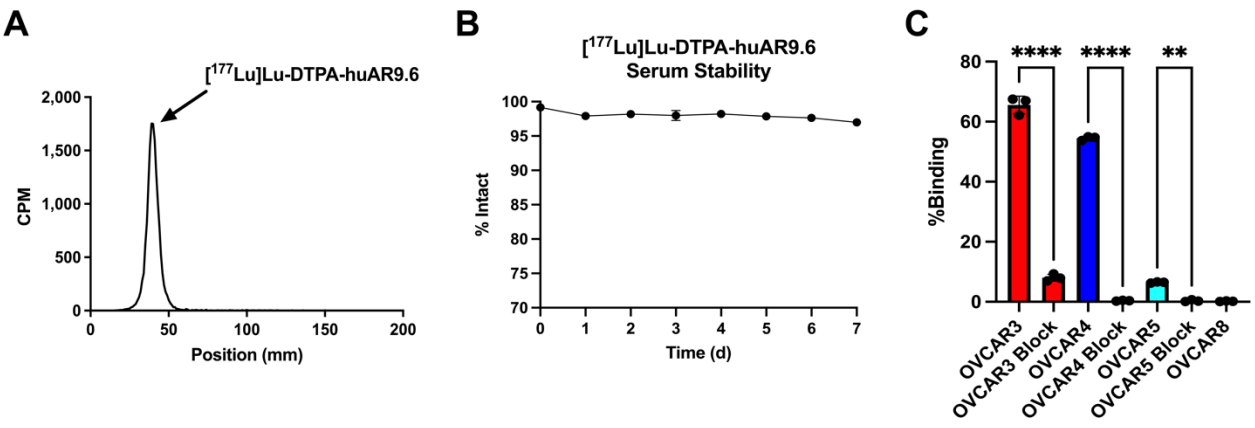

Supplemental Figure 14. *In vitro* characterization of [^{177}Lu]Lu-CHX-A"-DTPA-huAR9.6. (A) Radio-instant thin layer chromatography of [^{177}Lu]Lu-CHX-A"-DTPA-huAR9.6 showing high radiochemical purity > 99%. **(B)** [^{177}Lu]Lu-CHX-A"-DTPA-huAR9.6 shows >95% stability in human serum over 7 days at 37ºC. **(C)** [^{177}Lu]Lu-CHX-A"-DTPA-huAR9.6 shows high and specific binding in OVCAR3, OVCAR4, OVCAR5, & OVCAR8 cells. Binding is blockable with a 1000-fold excess of unlabeled huAR9.6. **P*-value ≤ 0.05, ***P*-value ≤ 0.01, ****P*-value ≤ 0.001, *****P*-value ≤ 0.0001.

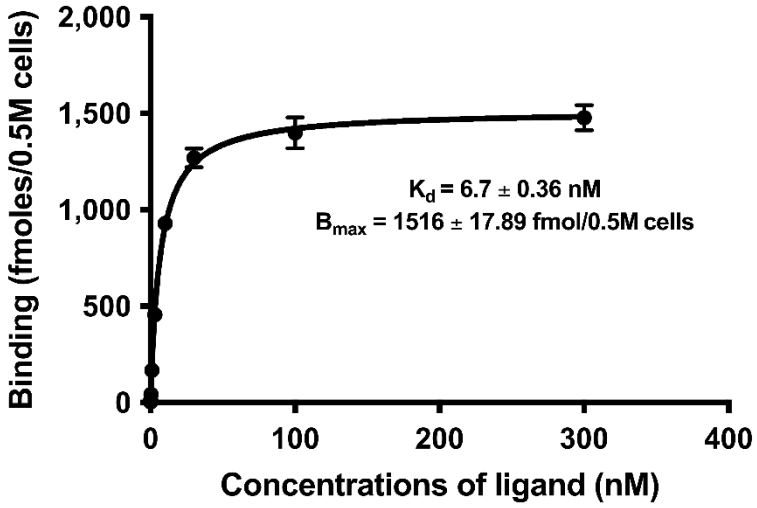

Supplemental Figure 15. Saturation binding curve of [^{177}Lu]Lu-CHX-A"-DTPA-huAR9.6 to OVCAR3 cells. PRISM v10 was used to calculate the B_{max} of 1516 ± 17.89 femtomoles/0.5M cells and a K_d of 6.7 ± 0.36 nM.

A

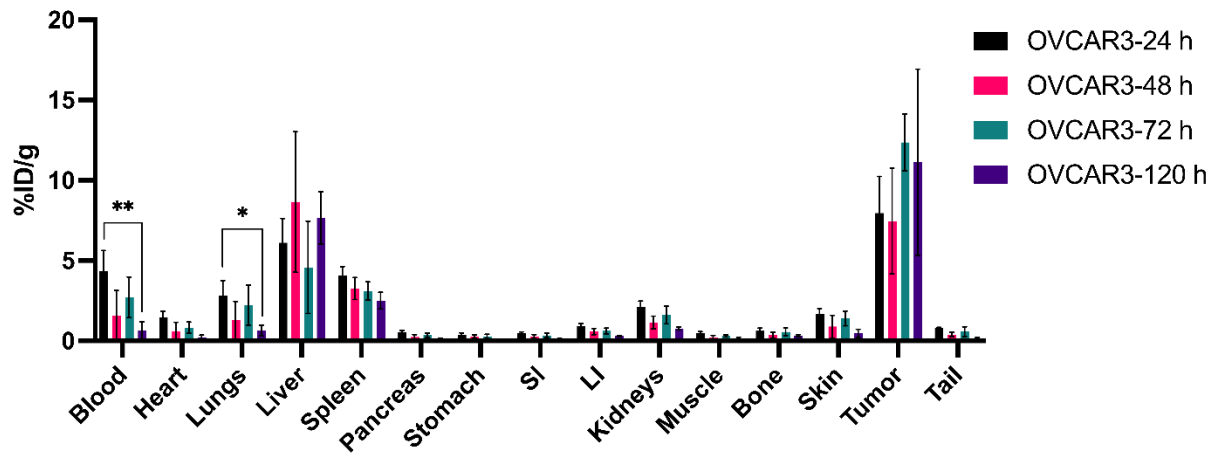

B

Time (p.i.) / Tissues	24 h (n=4)	48 h (n=4)	72 h (n=4)	96 h (n=4)	120 h (n=4)	144 h (n=4)
Blood	4.33 ± 1.28	1.58 ± 1.57	2.71 ± 1.26	1.51 ± 1.59	0.64 ± 0.55	0.91 ± 0.28
Heart	1.43 ± 0.41	0.59 ± 0.56	0.83 ± 0.35	0.48 ± 0.49	0.21 ± 0.15	0.35 ± 0.12
Lungs	2.83 ± 0.93	1.30 ± 1.17	2.22 ± 1.26	1.15 ± 1.15	0.64 ± 0.33	0.88 ± 0.16
Liver	6.11 ± 1.52	8.65 ± 4.37	4.58 ± 2.88	5.32 ± 3.00	7.67 ± 1.63	4.46 ± 1.38
Spleen	4.07 ± 0.56	3.30 ± 0.69	3.11 ± 0.57	2.98 ± 0.94	2.51 ± 0.52	2.30 ± 0.74
Pancreas	0.53 ± 0.11	0.23 ± 0.16	0.36 ± 0.13	0.20 ± 0.18	0.10 ± 0.06	0.16 ± 0.06
Stomach	0.36 ± 0.14	0.27 ± 0.10	0.28 ± 0.13	0.40 ± 0.47	0.09 ± 0.04	0.19 ± 0.04
Small Intestine	0.48 ± 0.08	0.27 ± 0.12	0.34 ± 0.13	0.25 ± 0.19	0.11 ± 0.04	0.15 ± 0.04
Large Intestine	0.93 ± 0.14	1.14 ± 0.40	0.62 ± 0.17	0.34 ± 0.08	0.31 ± 0.04	0.27 ± 0.06
Kidneys	2.11 ± 0.36	0.18 ± 0.15	1.61 ± 0.55	1.04 ± 0.47	0.77 ± 0.09	0.77 ± 0.09
Muscle	0.49 ± 0.08	0.35 ± 0.18	0.31 ± 0.07	0.23 ± 0.09	0.15 ± 0.07	0.22 ± 0.06
Bone	0.63 ± 0.17	0.89 ± 0.71	0.57 ± 0.24	0.47 ± 0.25	0.33 ± 0.06	0.44 ± 0.07
Skin	1.69 ± 0.32	0.89 ± 0.71	1.40 ± 0.45	0.79 ± 0.68	0.47 ± 0.26	0.68 ± 0.11
Tumor	7.95 ± 2.29	7.46 ± 3.29	12.35 ± 1.76	10.15 ± 6.99	11.12 ± 5.81	14.69 ± 3.38
Tail	0.80 ± 0.05	0.40 ± 0.14	0.57 ± 0.30	0.35 ± 0.21	0.17 ± 0.03	0.24 ± 0.04

Supplemental Figure 16. Full *ex vivo* biodistribution data after lateral tail vein injection of [^{177}Lu]Lu-CHX-A"-DTPA-huAR9.6 in OVCAR3 tumor-bearing R2G2 mice (3 µg, 1.11–1.30 MBq). **(A)** Percent injected dose per gram (%ID/g) 24-, 48-, 72-, and 120-hour timepoints. **(B)** Tabulated *ex vivo* biodistribution data. Expressed as mean percent injected dose per gram (%ID/g ± SD). **P*-value ≤ 0.05, ***P*-value ≤ 0.01, ****P*-value ≤ 0.001, *****P*-value ≤ 0.0001.

A

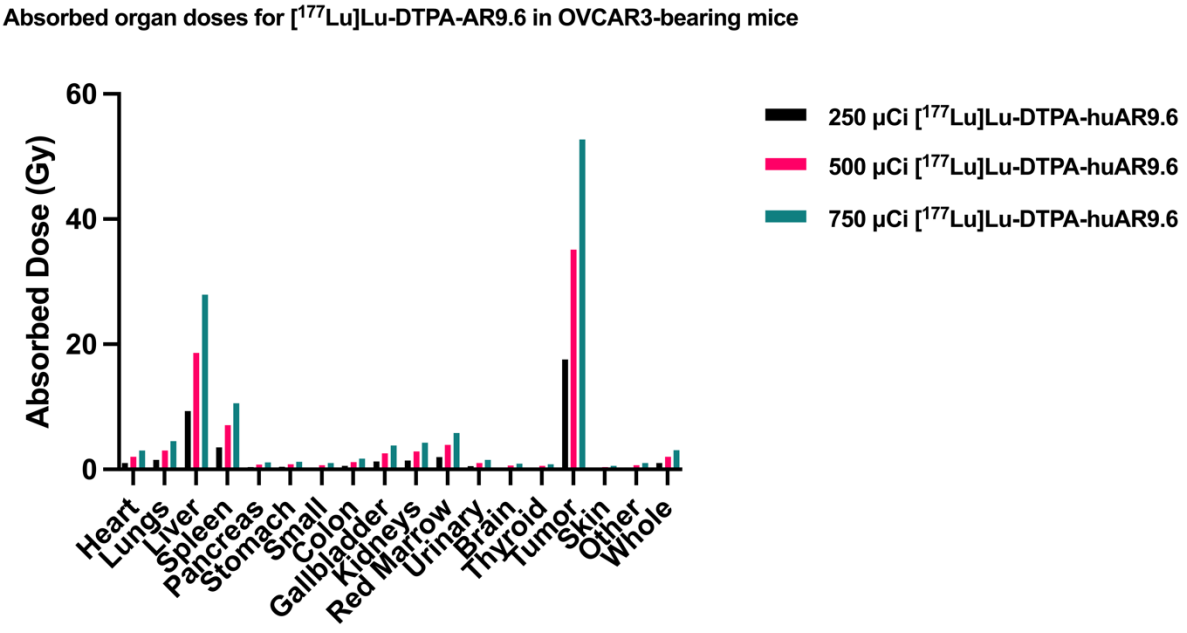

B

Organ	Gy @ 250 µCi AA	Gy @ 500 µCi AA	Gy @ 750 µCi AA	Therapeutic index
Heart	1.01	2.01	3.02	17.5
Lungs	1.50	3.00	4.51	11.7
Liver	9.31	18.63	27.94	1.9
Spleen	3.53	7.07	10.60	5.0
Pancreas	0.38	0.76	1.14	46.2
Stomach	0.41	0.83	1.24	42.5
Small intestine	0.34	0.69	1.03	51.1
Colon	0.58	1.16	1.74	30.3
Gallbladder	1.28	2.56	3.83	13.8
Kidneys	1.42	2.85	4.27	12.3
Red marrow	1.95	3.90	5.85	9.0
Urinary bladder	0.51	1.02	1.53	34.5
Brain	0.30	0.61	0.91	57.8
Thyroid	0.28	0.56	0.84	62.7
Tumor	17.57	35.14	52.71	--
Skin	0.19	0.38	0.57	92.8
Other tissues	0.33	0.66	1.00	52.9
Whole body	1.02	2.05	3.07	17.2

Supplemental Figure 17. (A) Calculated organ-level absorbed doses in OVCAR3 xenografted mice using [^{177}Lu]Lu-CHX-A"-DTPA-huAR9.6 biodistribution data. **(B)** Tabulated absorbed dose values and therapeutic indices, representing tumor-to-organ absorbed dose ratios.

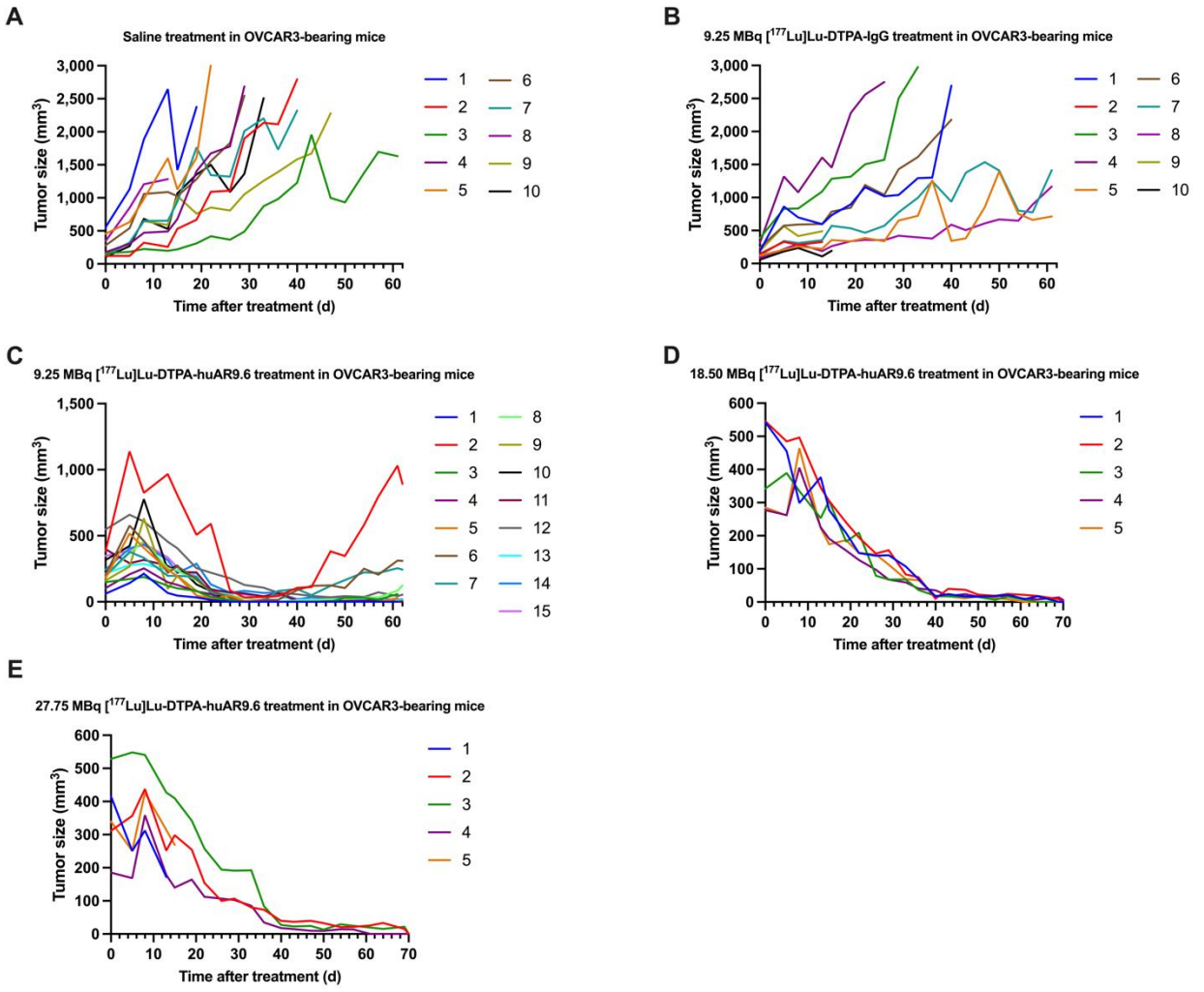

Supplemental Figure 18. Individual mouse tumor volumes for R2G2 OVCAR3 tumor-bearing mice in the **(A)** saline (150 µL/mouse via tail vein), **(B)** 9.25 MBq of [^{177}Lu]Lu-CHX-A"-DTPA-IgG (60 µg), **(C)** 9.25 MBq of [^{177}Lu]Lu-CHX-A"-DTPA-huAR9.6 (60 µg) **(D)** 18.5 MBq of [^{177}Lu]Lu-CHX-A"-DTPA-huAR9.6 (60 µg via tail vein) **(E)** 27.75 MBq of [^{177}Lu]Lu-CHX-A"-DTPA-huAR9.6 (60 µg) show a dose-dependent decrease in weight.

Supplemental Figure 19. Representative H&E **(A)** and immunohistochemistry **(B)** images of a recurrent OVCAR3 tumor from mouse #12 after a single dose of [^{177}Lu]Lu-CHX-A"-DTPA-huAR9.6. Immunohistochemistry image shows high MUC16 expression after staining with the huAR9.6 antibody.

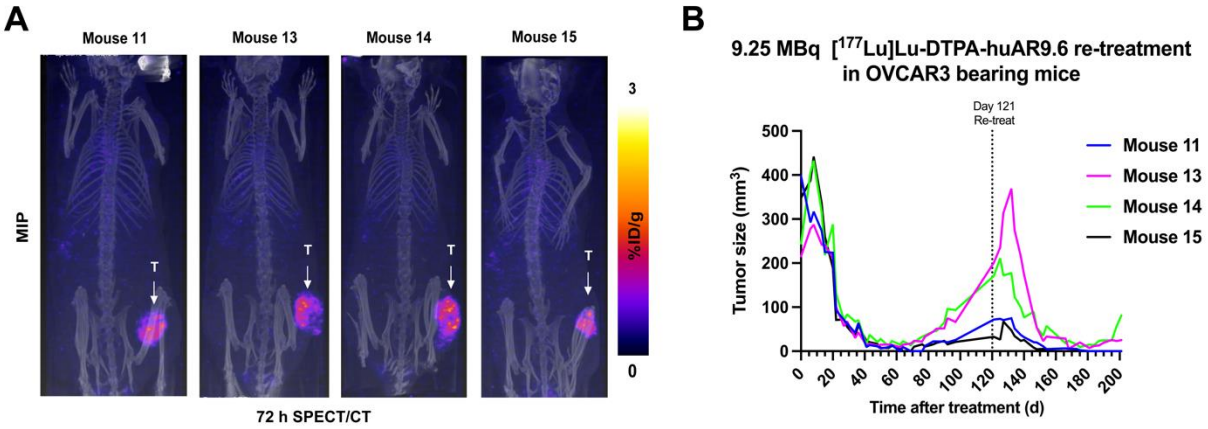

Supplemental Figure 20. [^{177}Lu]Lu-CHX-A"-DTPA-huAR9.6 still shows strong anti-tumor effects in recurrent tumors. (A) 72 h SPECT image of mice re-injected with [^{177}Lu]Lu-CHX-A"-DTPA-huAR9.6 showing uptake in the recurrent tumor (T) (**B**). Individual tumor volume (mm^3) growth curves of OVCAR3-bearing mice with recurring tumors. Images are represented as maximum intensity projections (MIPs).

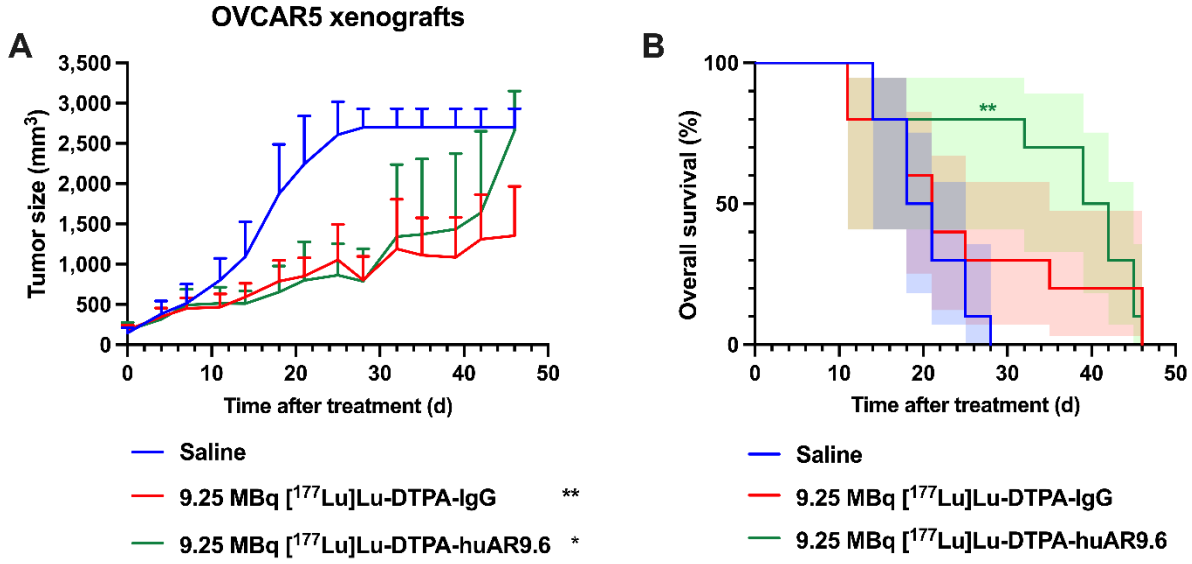

Supplemental Figure 21. [^{177}Lu]Lu-CHX-A"-DTPA-huAR9.6 treatment improves overall survival in OVCAR5-bearing mice. Overall survival percentage **(A)** and tumor volume (mm^3) growth curves of R2G2 OVCAR5-bearing mice **(B)**. Significant tumor growth inhibition was observed in the treated mice in comparison to saline control. Shading represents 95% confidence interval; *P-value ≤ 0.05, **P-value ≤ 0.01, ***P-value ≤ 0.001, ****P-value ≤ 0.0001; Mantel-Cox test.

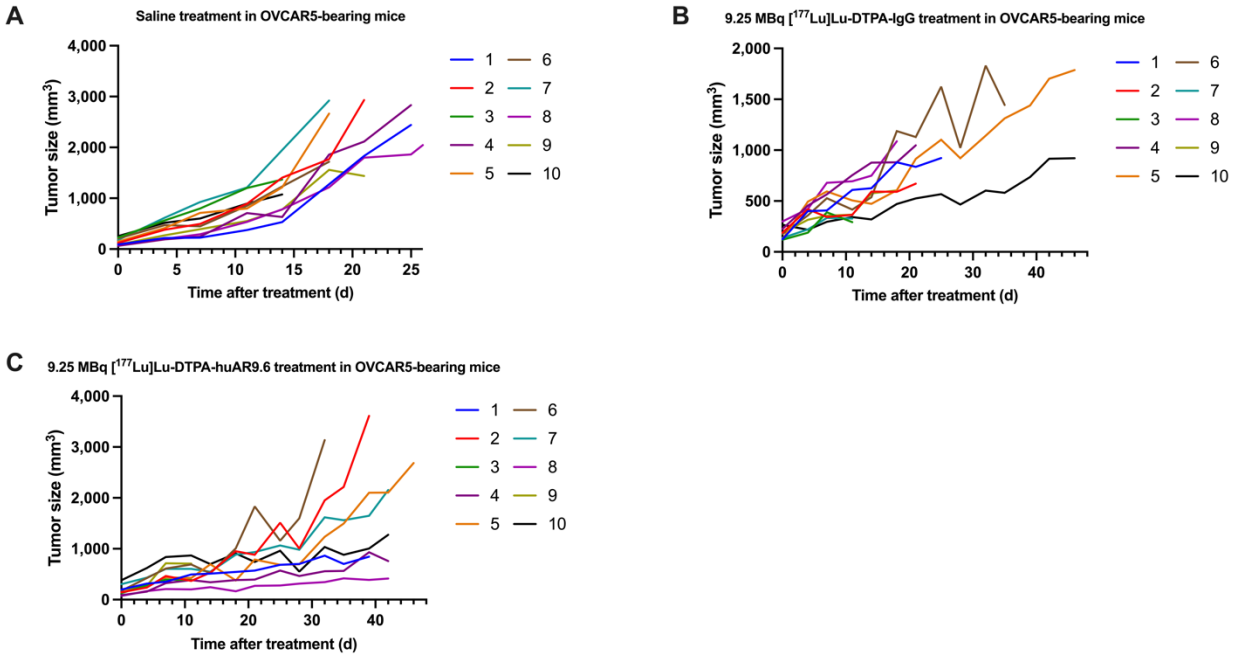

Supplemental Figure 22. Individual mouse tumor volumes for R2G2 OVCAR5 tumor-bearing mice in the **(A)** saline (150 µL/mouse), **(B)** 9.25 MBq of [^{177}Lu]Lu-CHX-A"-DTPA-IgG (60 µg), and **(C)** 9.25 MBq of [^{177}Lu]Lu-CHX-A"-DTPA-huAR9.6 (60 µg) cohorts.

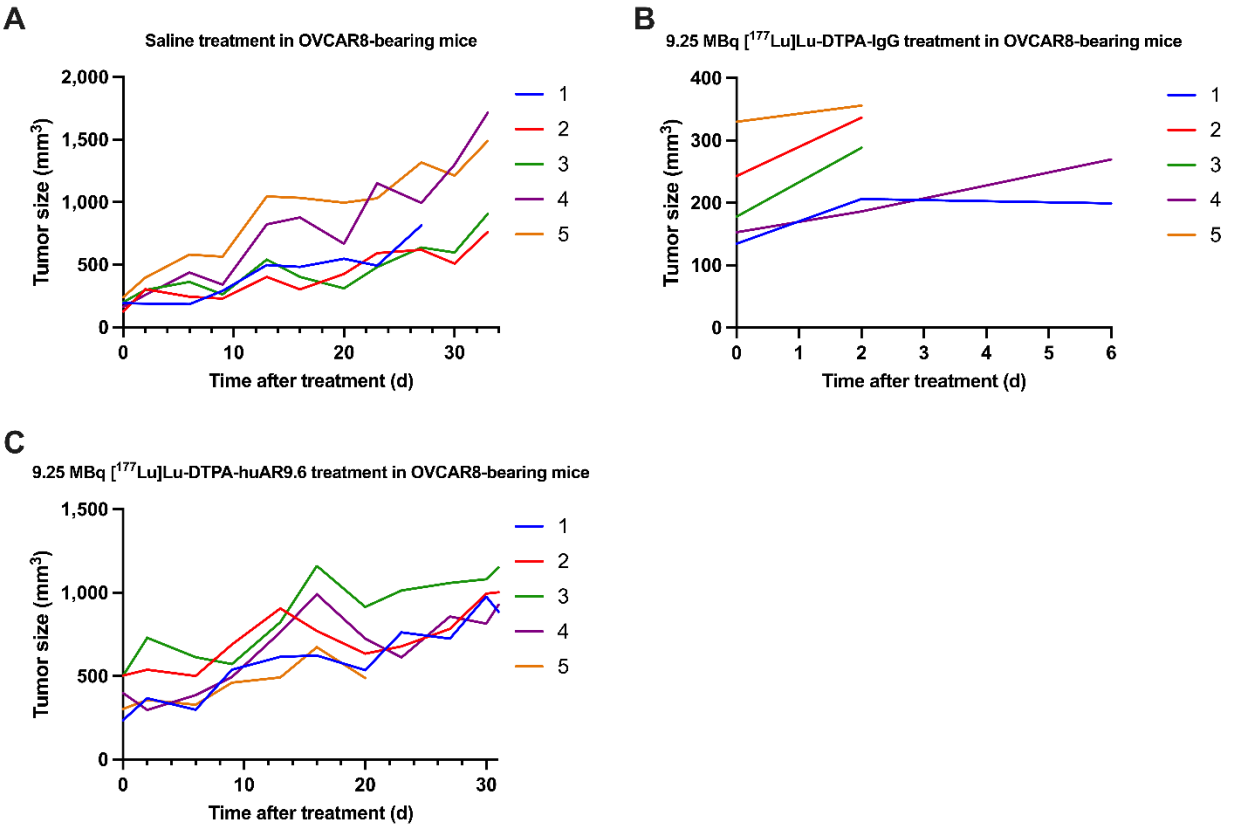

Supplemental Figure 23. Individual mouse tumor volumes for R2G2 OVCAR8 tumor-bearing mice in the **(A)** saline (150 µL/mouse), **(B)** 9.25 MBq of [^{177}Lu]Lu-CHX-A"-DTPA-IgG (60 µg), and **(C)** 9.25 MBq of [^{177}Lu]Lu-CHX-A"-DTPA-huAR9.6 (60 µg) cohorts.

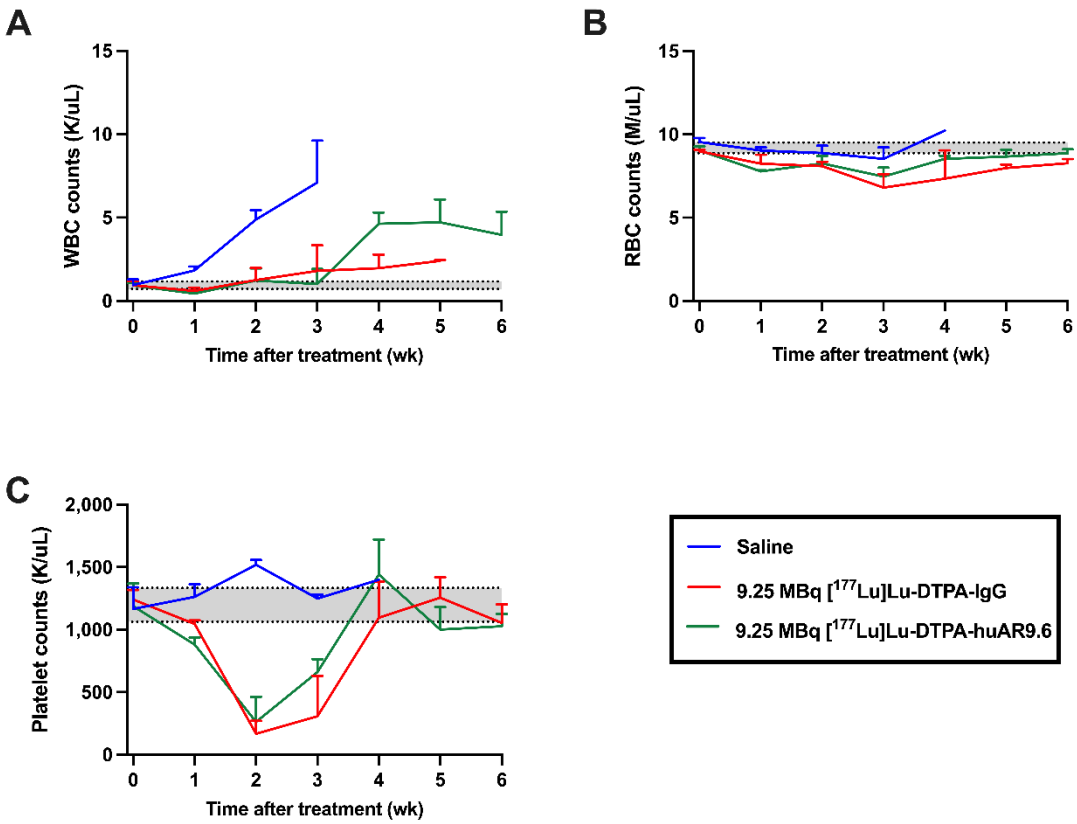

Supplemental Figure 24. White blood cell (WBC) (**A**), red blood cell (RBC) (**B**), and platelet (**C**) counts in OVCAR5 tumor-bearing mice for saline, [^{177}Lu]Lu-CHX-A"-DTPA-IgG, and [^{177}Lu]Lu-CHX-A"-DTPA-huAR9.6 groups. Three of the twenty parameters measured are shown. Gray shading indicates the mean ±1 SD of values collected from the entire cohort of OVCAR5-bearing mice prior to therapy initiation (week 0).

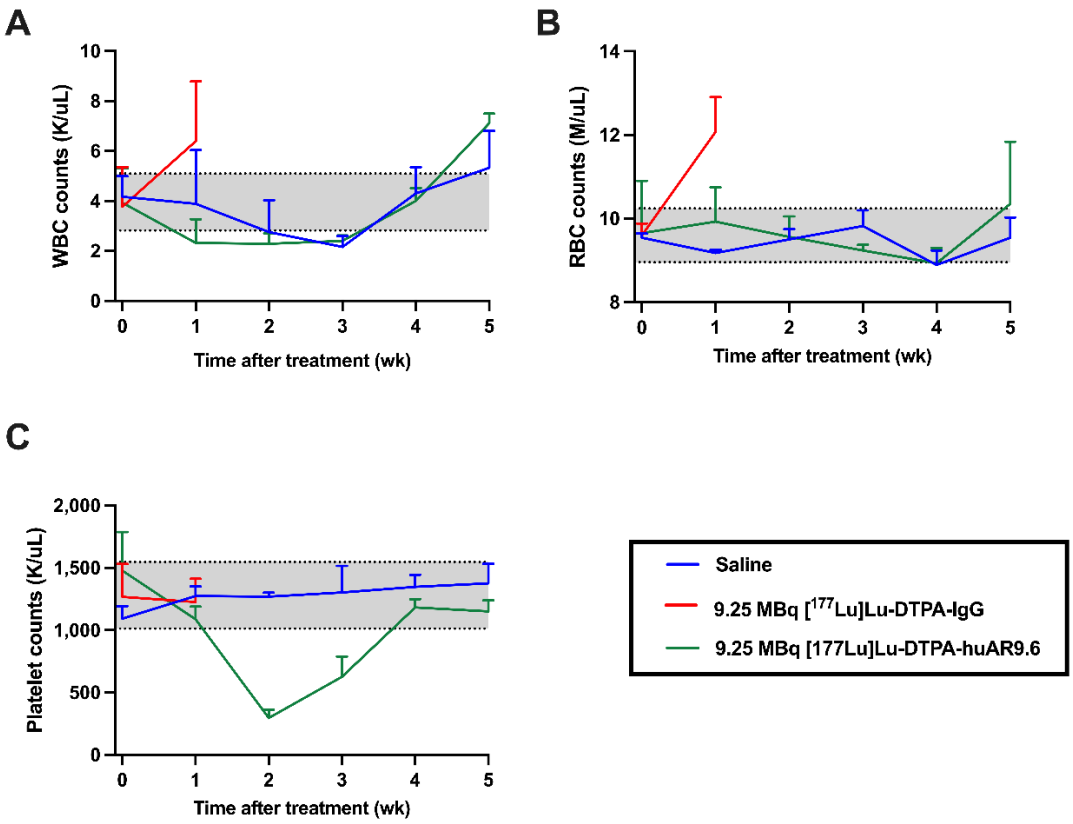

Supplemental Figure 25. White-blood cell (WBC) (**A**), red-blood cell (RBC) (**B**), and platelet (**C**) counts in OVCAR8 tumor-bearing mice for saline, [^{177}Lu]Lu-CHX-A"-DTPA-IgG, and [^{177}Lu]Lu-CHX-A"-DTPA-huAR9.6 groups. Three of the twenty parameters measured are shown. Gray shading indicates the mean ±1 SD of values collected from the entire cohort of OVCAR8-bearing mice prior to therapy initiation (week 0).

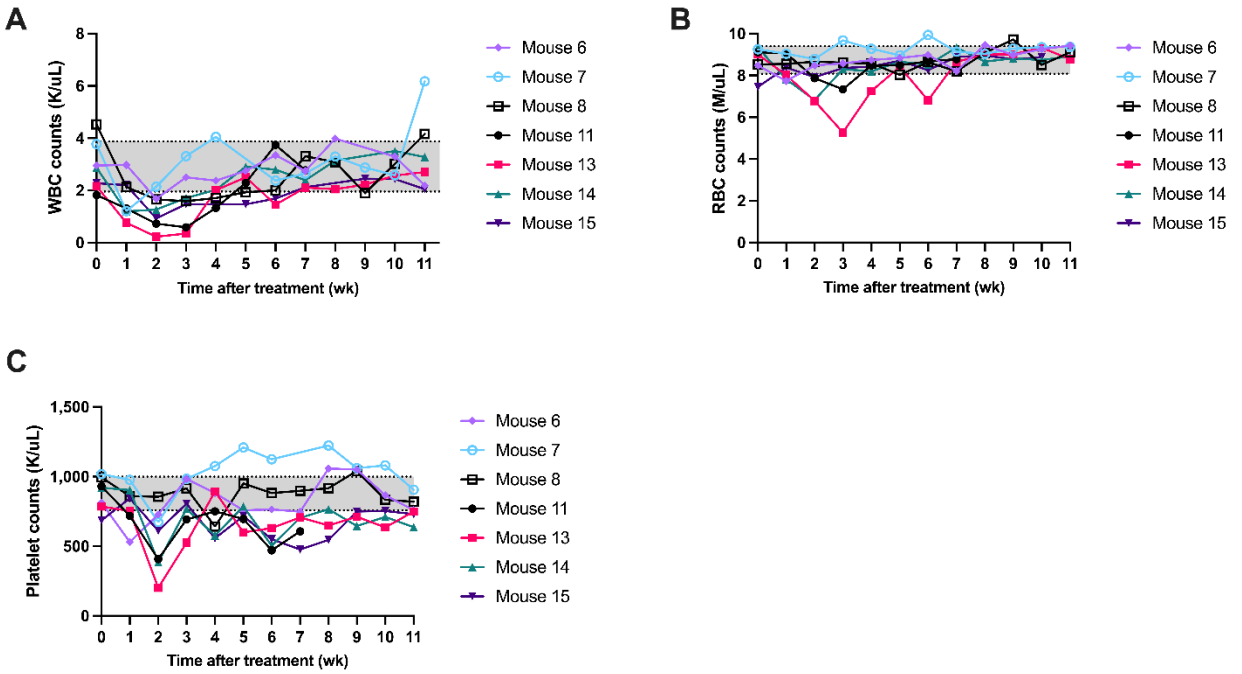

Supplemental Figure 26. White-blood cell (WBC) (**A**), red-blood cell (RBC) (**B**), and platelet (**C**) counts in OVCAR3 tumor-bearing mice re-treated with 9.25 MBq of [^{177}Lu]Lu-CHX-A"-DTPA-huAR9.6. Three of the twenty parameters measured are shown. Gray shading indicates the mean ±1 SD of values collected from the entire cohort of OVCAR3-bearing mice prior to therapy initiation (week 0).

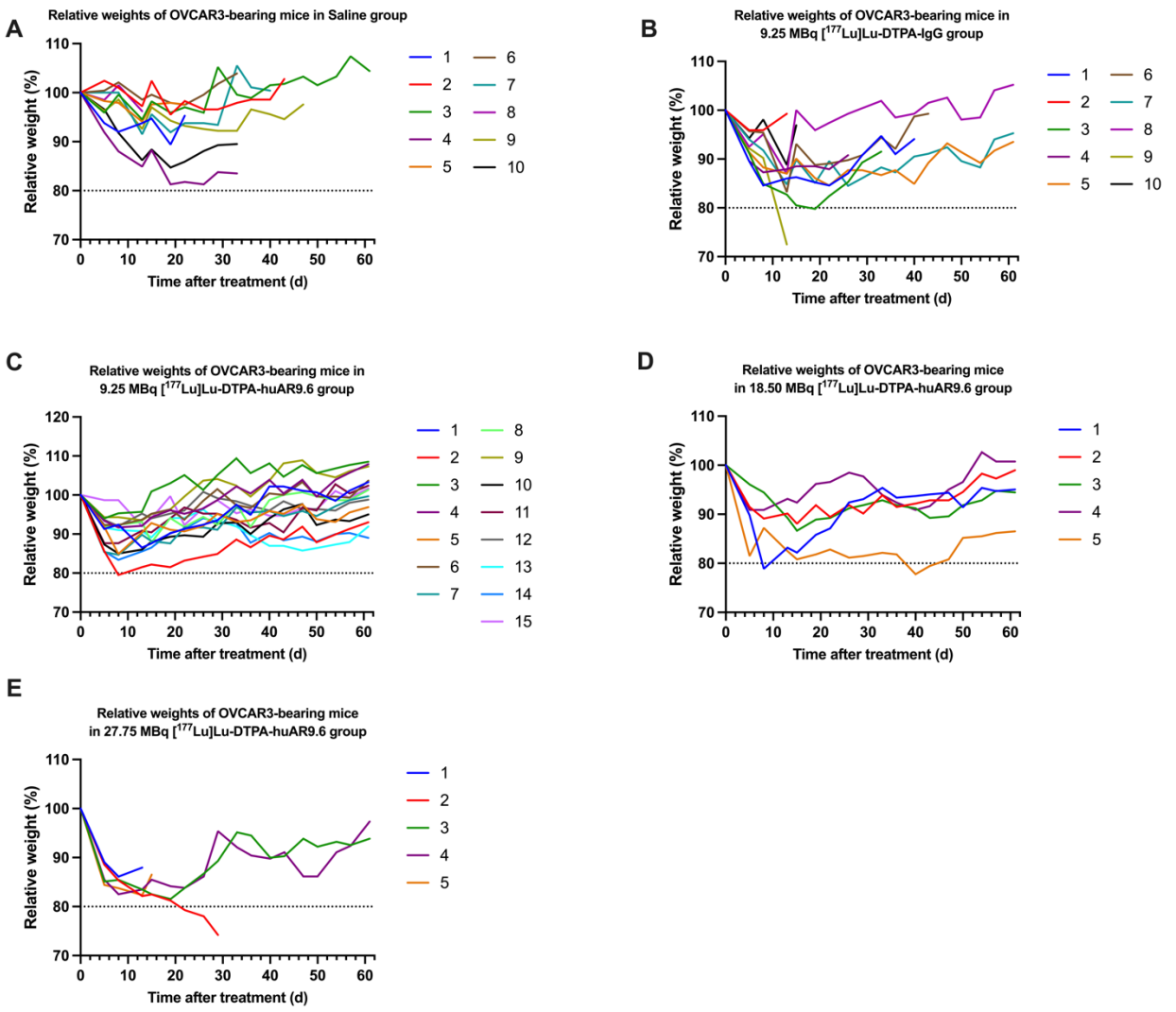

Supplemental Figure 27. Individual relative weight percentages for OVCAR3 tumor-bearing mice after a single dose of **(A)** saline (150 µL/mouse), **(B)** 9.25 MBq of [^{177}Lu]Lu-CHX-A"-DTPA-IgG (60 µg), **(C)** 9.25 MBq of [^{177}Lu]Lu-CHX-A"-DTPA-huAR9.6 (60 µg) **(D)** 18.5 MBq of [^{177}Lu]Lu-CHX-A"-DTPA-huAR9.6 (60 µg) **(E)** 27.75 MBq of [^{177}Lu]Lu-CHX-A"-DTPA-huAR9.6 (60 µg). Data shows a dose-dependent decrease in weight.

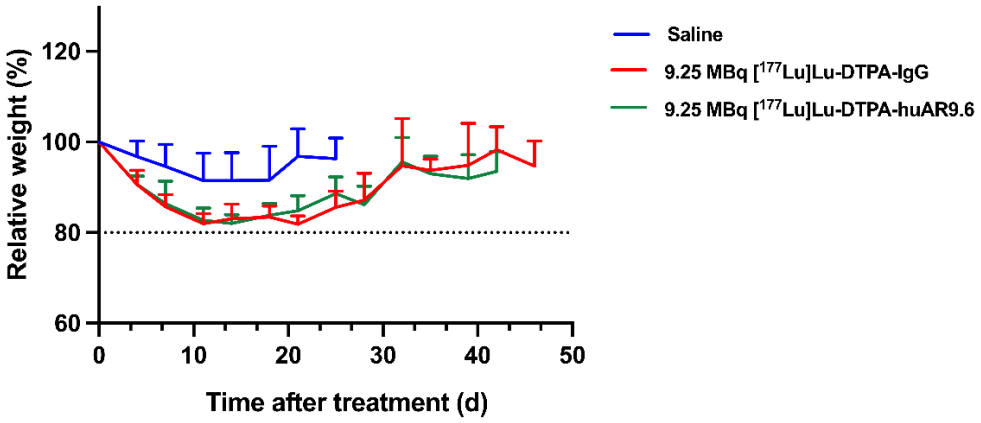

Supplemental Figure 28. Mean relative weight percentages for OVCAR5 tumor-bearing mice in each cohort.

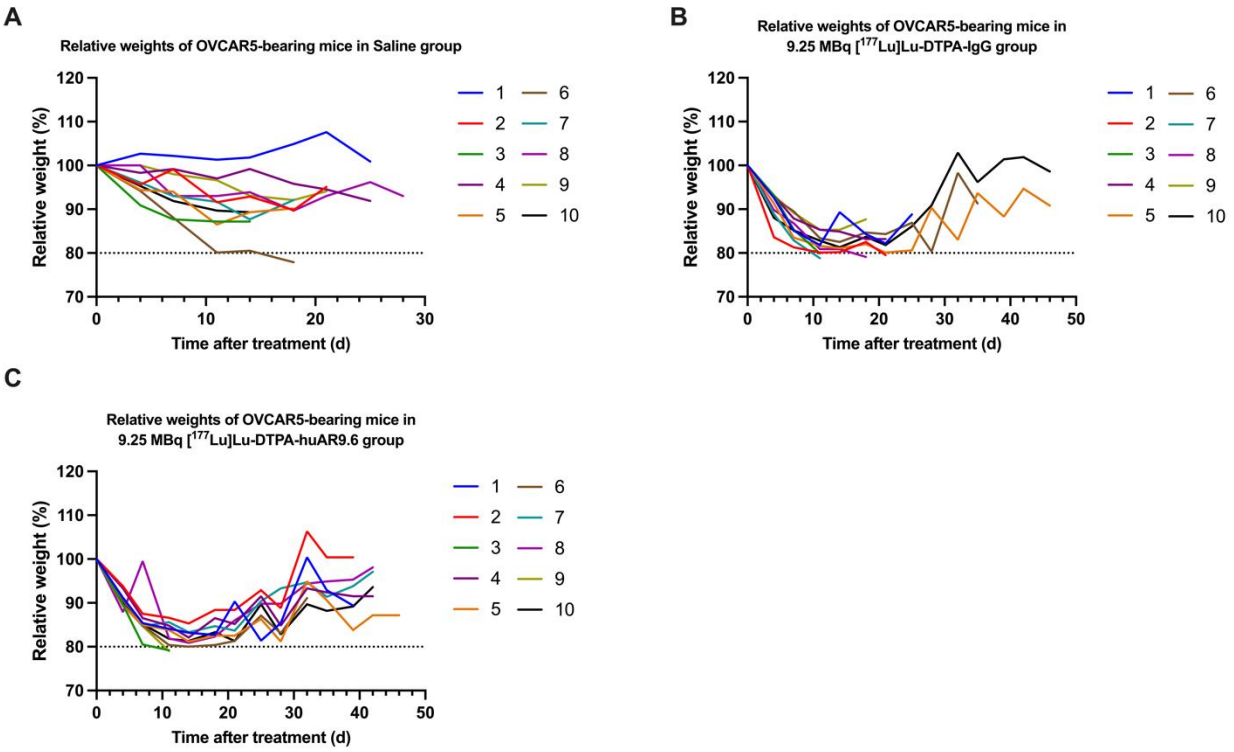

Supplemental Figure 29. Individual mouse relative weight percentages for R2G2 OVCAR5 tumor-bearing mice in the **(A)** saline (150 µL/mouse) **(B)** 9.25 MBq of [^{177}Lu]Lu-CHX-A"-DTPA-IgG (60 µg), and **(C)** 9.25 MBq of [^{177}Lu]Lu-CHX-A"-DTPA-huAR9.6 (60 µg) cohorts.